Structure, Vol. 11, 155–164, February, 2003, ©2003 Elsevier Science Ltd. All rights reserved. PII S0969-2126(02)00943-7

Solution Structure of the MAPK Phosphatase PAC-1 Catalytic Domain: Insights into Substrate-Induced Enzymatic Activation of MKP

Amjad Farooq, Olga Plotnikova, Gaurav Chaturvedi, Sherry Yan, Lei Zeng, Qiang Zhang, and Ming-Ming Zhou*
Structural Biology Program
Department of Physiology and Biophysics
Mount Sinai School of Medicine
New York University
One Gustave L. Levy Place
New York, New York 10029

Summary

Inactivation of mitogen-activated protein kinases (MAPKs) by MAPK phosphatases (MKPs) is accomplished via substrate-induced activation of the latter enzymes; however, the structural basis for the underlying mechanism remains elusive. Here, we report the three-dimensional solution structure of the C-terminal phosphatase domain of the prototypical MKP PAC-1, determined when bound to phosphate. Structural and biochemical analyses reveal unique active site geometry of the enzyme important for binding to phosphorylated threonine and tyrosine of MAPK ERK2. Our study further demonstrates that the dynamic interaction between the N-terminal kinase binding domain and the C-terminal phosphatase domain of an MKP is directly coupled to MAPK-induced conformational change of the phosphatase active site, which is essential for eliciting its full enzymatic activity.

Introduction

Mitogen-activated protein kinases (MAPKs) play a pivotal role in controlling numerous cellular processes, including differentiation, mitogenesis, oncogenesis, and apoptosis [1–3]. The biological importance of MAPKs is underscored by tight control of their activation through dual phosphorylation of threonine and tyrosine in the activation loop [1–5] and their inactivation by a family of dual-specificity MAPK phosphatases (MKPs), many of which are encoded by early genes induced by MAPKs, thus forming a negative-feedback mechanism [6, 7]. All MKPs consist of two functional domains—an N-terminal kinase binding domain and a C-terminal phosphatase domain. Many MKPs exhibit distinct substrate specificity toward three major classes of MAPKs, i.e., extracellular signal-regulated kinases (ERK1/2), c-Jun N-terminal kinases/stress-activated protein kinases (JNK-1/2/3/SAPK), and p38 proteins (p38$\alpha/\beta/\gamma/\delta$) [8, 9]. For instance, PAC-1 that is expressed predominantly in hematopoietic cells was discovered by virtue of its specific inactivation of ERKs in T cell activation [10, 11], whereas MKP-3 and M3-6 are highly selective in inactivating ERKs or JNK/SAPK and p38 MAPKs, respectively [12–14]. This high substrate selectivity of MKPs is, in part, due to their ability to recognize distinctively different dual-phosphorylation sites containing the **pT-*X*-pY** motif, where pT and pY are phosphothreonine and phosphotyrosine and *X* is glutamate, proline, or glycine, respectively, in the three different classes of MAPKs.

Recent studies have shown that direct binding of the N-terminal kinase binding domains to selective MAPKs also contributes to the substrate specificity of MKPs [15–19]. More strikingly, this direct enzyme-substrate interaction results in catalytic activation of MKP-3 [16], which otherwise exhibits very low phosphatase activity in the absence of substrates. Structural and biochemical studies of MKP-3 have further demonstrated that the enzyme utilizes a conserved ***XX*RR*XX*K*XX*L*X*V** motif in its N-terminal kinase binding domain for specific interaction with ERK2 [20–23] and that MKP-3 activity is controlled by a mechanism of substrate-induced activation, rather than autoinhibition [20, 24, 25]. The latter mechanism is seen in the SHP-2 tyrosine phosphatase [26]. Collectively, these studies suggest that MKP-3 binding to ERK2 allosterically causes conformational rearrangement of the C-terminal phosphatase domain, leading to its catalytic activation [16, 20]. This hypothesis seems consistent with the three-dimensional crystal structure of the free MKP-3 phosphatase domain, which shows that the key catalytic residues at the active site are structurally disengaged for catalysis [27].

Despite these important advances, major questions regarding the structural basis of substrate recognition and the mechanism of substrate-induced catalytic activation of MKPs remain unanswered. For instance, do dual-specificity MKPs interact with phosphothreonine and phosphotyrosine in the activation loop of an MAPK simultaneously? What amino acid residues flanking phosphothreonine and phosphotyrosine in MAPKs are specifically recognized by MKPs? How does an MAPK binding by an MKP affect conformational rearrangement of the phosphatase active site, which results in its catalytic activation? In an effort to address these questions, we have determined the three-dimensional solution structure of the C-terminal phosphatase domain from the prototypical MKP PAC-1 using nuclear magnetic resonance (NMR) spectroscopy. We have further investigated the structural basis of its substrate recognition and interdomain interaction with the conserved N-terminal kinase binding domain. Our findings provide new insights into the structural and functional relationships of MKPs.

Results and Discussion

Structure Determination

To conduct the NMR structural analysis, we substituted the enzymatic nucleophile C257 with serine for the C-terminal phosphatase domain of human PAC-1 (Figures 1A and 1B). Mutation of the equivalent cysteine to

*Correspondence: zhoum@inka.mssm.edu

Key words: MAPK dephosphorylation; MKP phosphatase domain; PAC-1; enzymatic activation; NMR structure

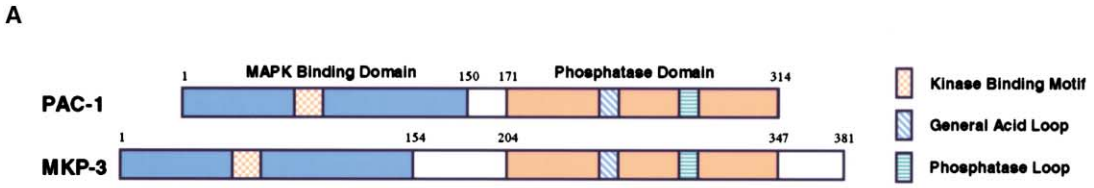

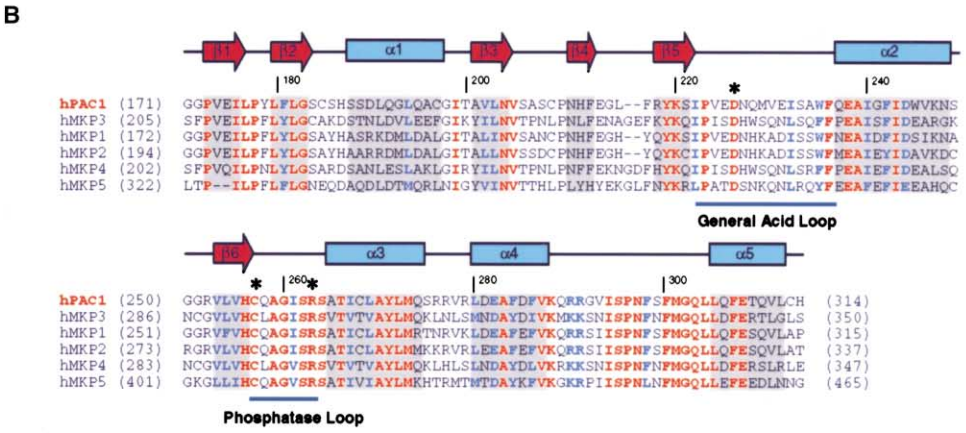

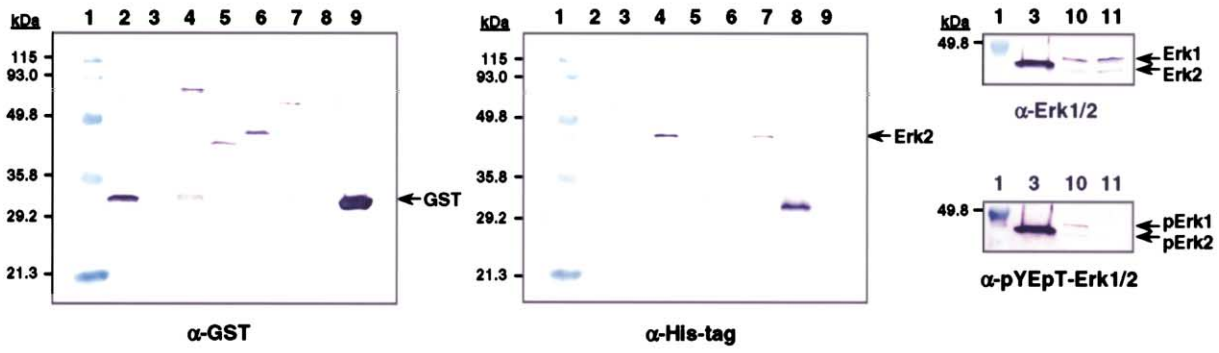

1. MW
2. GST alone + His-tagged pY/pT-Erk2
3. His-tagged pY/pT-Erk2
4. GST-MKP3 (aa 1-384) + pY/pT-Erk2
5. GST-PAC1 (aa 170-314) + pY/pT-Erk2
6. GST-PAC1 (aa 127-314) + pY/pT-Erk2
7. GST-PAC1 (aa 1-314) + pY/pT-Erk2
8. His-tagged Shc PTB domain
9. GST
10. PC12 cell extracts treated with NGF (+control)
11. PC12 cell extracts without NGF treatment (-control)

Figure 1. Functional Domains of MKPs

(A) Domain organization of PAC-1 and MKP-3. N-terminal kinase binding domain, blue; C-terminal phosphatase domain, orange. Numerals indicate domain boundaries based on the structural analysis. The functionally important sequences, including the kinase interaction motif, the general acid loop, and the phosphatase active site loop, are highlighted with shaded boxes.

(B) Sequence alignment of the phosphatase domains. Absolutely conserved residues, red; highly conserved residues, blue. Sequence numbers are indicated along the protein sequences. Secondary structures of the PAC-1 phosphatase domain are shown as colored rectangles (α helices) and arrows (β strands). Asterisks highlight the PAC-1 catalytic residues, i.e., D226, C257, and R263. Note that the enzymatic nucleophile C257 of PAC-1 was changed to serine in the NMR study.

(C) GST pull-down study of PAC-1 and ERK2 interaction. Western blot with anti-GST antibodies shows binding of the GST fusion PAC-1 and MKP3 proteins immobilized on the GST Sepharose beads (left panel). The middle panel depicts Western blot with anti-hisidtine tag antibodies,

serine in protein tyrosine phosphatases has been shown to abrogate catalytic activity, but to retain substrate recognition [28, 29], making it feasible for studying the enzyme-substrate complex. This mutation in PAC-1 did not cause any significant structural perturbation of the protein, as judged by NMR spectral analysis. To investigate the feasibility of structural determination of an enzyme-substrate complex, we performed NMR binding of the phosphatase domain with phosphorylated peptides derived from the ERK2 activation loop (residues 175–193, DHDHTGFL**pTEpY**VATRWYRA). Surprisingly, both NMR titration and intermolecular NOE experiments revealed that the PAC-1 protein, composed of residues 170–314 or 127–314, did not form a stable complex with either mono- or bis-phosphorylated ERK2 peptide. Specifically, at 1:1 protein-peptide molar ratio, backbone amide resonances of the protein in the ^{15}N-HSQC spectrum showed negligible chemical shift perturbations, as compared to the free form spectrum. Even when the peptide concentration was increased to a 1:10 protein-peptide molar ratio (with ~5 mM peptide), resonance perturbation of the protein was still very small and limited to a few residues (data not shown). NMR titration with a shorter ERK2 peptide (residues 177–189, DHTGFL**pTEpY**VATR), in its mono- or bis-phosphorylated form, showed similarly weak interactions with the phosphatase domain. As NMR can detect weak, but specific, protein-ligand interactions (K_d of μM to mM), these observations may be explained by two reasons: (1) the synthetic ERK2 peptide loses its geometric conformation adopted in the ERK2 protein that is required for enzyme-substrate binding, and (2) the active site conformation of the phosphatase domain alone is altered as compared with the full-length PAC-1 and, thus, not suited for stable enzyme-substrate complex formation.

To test these possibilities, we performed an in vitro binding assay using recombinant and purified GST fusion PAC-1 and dual-phosporylated ERK2 proteins. As shown in Figure 1C, the phosphatase domain of PAC-1 (residues 170–314 or 127–314) exhibited no detectable binding to ERK2 (lanes 5 and 6), whereas binding of the full-length PAC-1 to ERK2 was comparable to that of MKP-3 (lanes 4 and 7). These results substantiate our NMR titration results and argue that the active site conformation of the phosphatase domain of PAC-1, in the absence of the kinase binding domain, is not optimal for substrate recognition and that the full-length PAC-1-ERK2 association results from the phosphatase domain binding to the dual-phosphorylation site in ERK2 and/or the kinase binding domain interaction with ERK2 in regions other than the phosphorylation site.

While the phosphatase domain does not bind to the ERK2 peptide, it interacts with phosphate, which is a competitive inhibitor for the enzyme. Interestingly, the protein gives rise to excellent NMR spectra in a buffer containing low, but not high, phosphate concentration (see below); stability of the protein was dramatically increased in the presence of phosphate. These promising results prompted us to determine the three-dimensional structure of the phosphatase domain of PAC-1 (residues 170–314) in a 5 mM phosphate buffer of pH 6.5. The phosphatase domain, determined with a total of 2374 NMR-derived distance and dihedral angle restraints [30], adopts a compact tertiary structure (Figure 1B). An ensemble of the 20 lowest-energy NMR structures and a ribbon diagram of the average minimized structure are depicted in Figures 2A and 2B. Excluding a flexible α4–α5 loop (residues 288–304), the NMR structures are well defined (Table 1).

Structure of the Phosphatase Domain

The PAC-1 phosphatase domain contains an α/β structure, consisting of a central six-stranded mixed β sheet with a folding topology of +1x, +2x, +2x, −1x, −2x that is sandwiched by four α helices on one side and one helix on the other (Figure 2B). The location of the enzyme active site is marked by the conserved phosphatase signature sequence **HCXXXXXR** (residues 256–263) in the β6–α3 loop (Figure 2C), where C257 is the enzymatic nucleophile and R263 coordinates with the phosphate group on phosphotyrosine or phosphothreonine. The conserved D226, which corresponds to D262 in MKP-3 and is believed to serve as a general acid by donating a proton to phenolic or hydroxyl oxygen of the leaving group of a substrate [31], resides in the so-called general acid loop connecting β5 and α2 (Figure 2C).

While the overall fold of the PAC-1 phosphatase domain structure is very similar to the structure of the MKP-3 phosphatase domain determined by X-ray crystallography [27], differences of structural elements do exist between the two structures (Figures 2C and 2D). For instance, α1, which is packed antiparallel to the central strands on one side of the β sheet in PAC-1, is one turn shorter in the crystal structure. Conversely, α4, which forms three turns in the crystal structure, has only two turns in the NMR structure, the latter of which is followed by a long and flexible α4–α5 loop. The relative orientation of α5 with respect to the active site helix α3 is also different—it is ~30° in the MKP-3 structure and ~75° in the PAC-1 structure. Another notable structural difference is the location of the β5–α2 loop, which contains the catalytically important residue D226. In the crystal structure of MKP-3, the equivalent D262 is disengaged from the other catalytic residues by over 10 Å. On the basis of this distinct structural feature, it was suggested that a major conformational rearrangement would have to take place in order to bring the catalytic residues together for full enzymatic activity in catalysis [27]. However, in PAC-1, the corresponding loop containing D226 appears closer to the phosphatase signature sequence (Figure 2C). This striking structural difference could be, in part, due to differences in the buffer conditions in the two structural studies (see below).

showing the relative amount of the ERK2 protein bound to PAC-1 and MKP3 proteins on the GST column in each binding experiment. The right panels are Western blots with anti-ERK1/2 or anti-ACTIVE ERK1/2 antibodies (Promega), demonstrating that the recombinant ERK2 protein used in this study was dual phosphorylated on T183 and Y185 in the activation loop. PC12 cell extracts with or without treatment of nerve growth factor (NGF) (lanes 10 and 11) (Promega) were used as positive or negative controls, respectively.

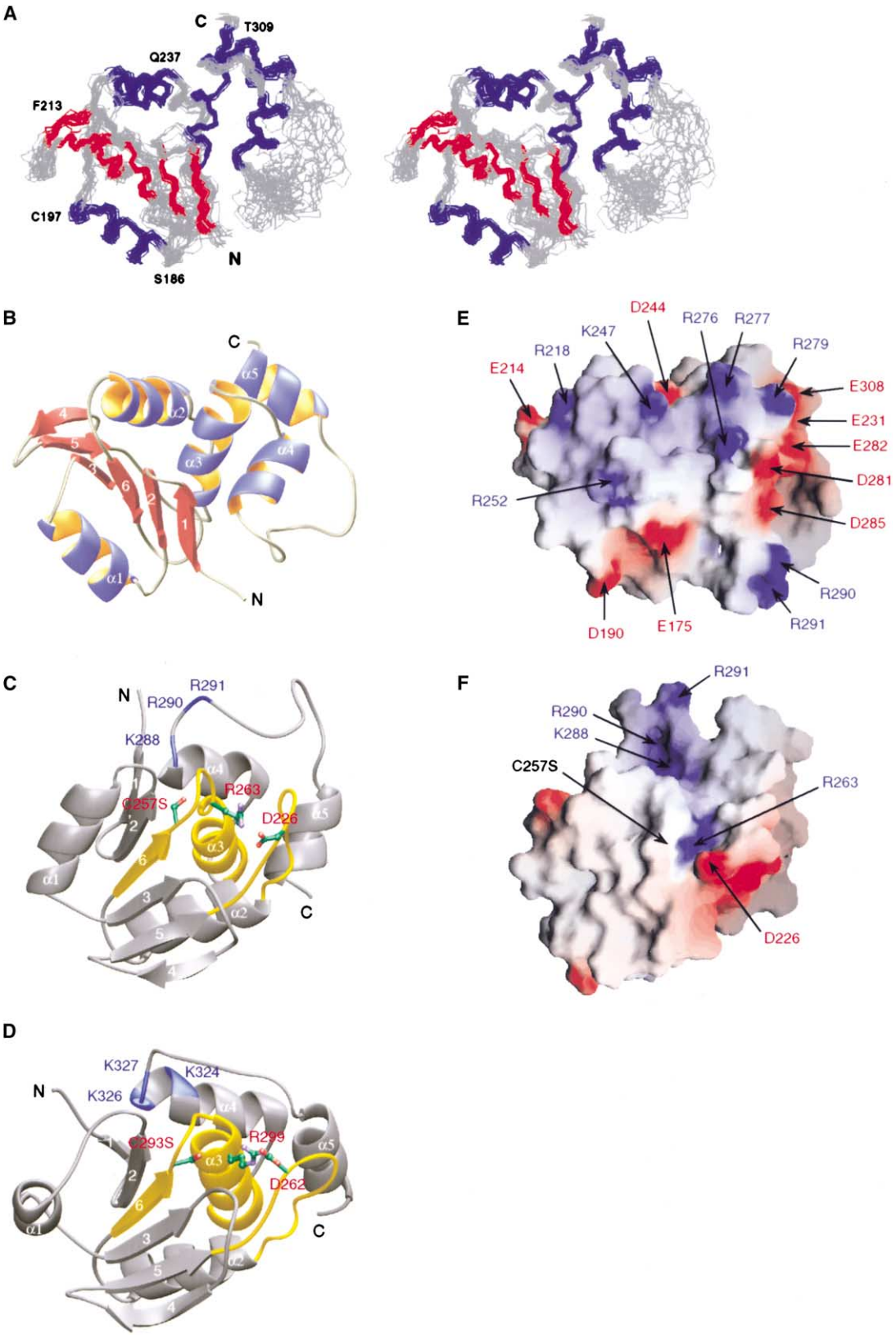

Figure 2. NMR Structure of the Phosphatase Domain of PAC-1

(A) Stereo view of the backbone atoms (N, C^{α}, and C') of 20 superimposed NMR-derived structures of the PAC-1 phosphatase domain (residues 170–314). Four N-terminal residues that are structurally disordered are omitted for clarity. The secondary-structural elements of α helices and β strands are colored in green and orange, respectively.

Table 1. NMR Structural Statistics of the PAC-1 Phosphatase Domain

Total experimental restraints	2374	
Total NOE distance restraints[a]	2138	
Ambiguous	173	
Unambiguous	1965	
Intraresidue ($i = j$)	768 (39.1%)	
Sequential ($\|i - j\| = 1$)	444 (22.6%)	
Medium ($2 \leq \|i - j\| \leq 4$)	339 (17.3%)	
Long range ($\|i - j\| > 4$)	414 (21.1%)	
Hydrogen bond restraints	110	
Dihedral angle restraints	126	
Final energies (kcal · mol^{-1})[b]		
E_{Total}	213.1 ± 16.2	
E_{NOE}	20.2 ± 6.1	
$E_{Dihedral}$	0.2 ± 0.1	
E_{L-J}	−644.2 ± 20.1	
Ramachandran Plot (%)	Full Molecule[c]	Secondary Structure[d]
Most-favorable region	71.3 ± 2.5	91.9 ± 3.0
Additionally allowed region	21.2 ± 2.6	8.1 ± 1.0
Generously allowed region	6.2 ± 2.0	0.0 ± 0.0
Disallowed region	1.4 ± 1.1	0.0 ± 0.0
Rmsd's of Atomic Coordinates (Å)		
Backbone	0.75 ± 0.09	0.51 ± 0.08
Heavy atoms	1.27 ± 0.10	0.99 ± 0.08

[a] Of the 2138 total NOE-derived distance restraints, 881 were obtained with the ARIA program, and 173 of those are classified as ambiguous NOEs. The latter resonance signals in the spectra match with more than one proton atom in both the chemical shift assignment and the final NMR structures.
[b] Based upon the 20 lowest-energy minimized structures. The Lennard-Jones potential was not used during any refinement stage. None of these final structures exhibit NOE-derived distance restraint violations greater than 0.5 Å or dihedral angle restraint violations greater than 5°.
[c] Residues 173–287 and 305–312.
[d] Residues 173–176, 180–183, 188–197, 201–204, 211–213, 218–221, 237–248, 253–256, 265–274, 280–287, and 305–312.

Analysis of surface electrostatic potential shows that the enzyme active site is located at one end of a surface-exposed channel lined by the α4–α5 loop on one side and the β2–α1 and β6–α3 loops as well as the interdomain linker sequence (N-terminal to β1) on the other side (Figures 2C and 2F). In addition to R263 at the active site, a group of positively charged residues, K288, R290, and R291, are clustered at the other end of this crevice, suggesting another binding site for the phosphorylated residue(s) in ERK2. The back surface of the enzyme, opposite to the active site (the front surface), is also distinctively polarized (Figure 2E). Surface-exposed residues R218, K247, R252, R276, R277, and R279 form a continuous and positively charged patch that is surrounded by a strip of negatively charged residues, including E175, D190, E231, D281, E282, D285, and E308. This distinctive structural feature suggests that this is a potential site for protein-protein interaction.

Substrate Binding

To characterize the active site, we conducted NMR titration of the phosphatase domain with small molecular substrate analogs. Remarkably, addition of phosphate causes extensive portions of the enzyme (more than just the active site region) to exhibit major backbone amide resonance changes (Figure 3A), implicating a global structural alteration. This phosphate-dependent global structural perturbation is possibly due to phosphate binding to more than just the active site and may explain the marked differences of the structural elements, i.e., the β5–α2 loop, between the NMR structure of PAC-1 and the crystal structure of MKP-3, which were determined in a 5 mM phosphate buffer of pH 6.5 and in a 100 mM Tris buffer of pH 8.2 containing 2.5 M NaCl, respectively.

Unexpectedly, the major perturbed residues upon addition of *p*-nitro-phenyl phosphate (*p*NPP), which mimics phosphotyrosine, are clustered mostly in α3, α4, and the β2–α1 loop instead of at the active site between β6 and α3 (Figure 3B). This result argues that the PAC-1 active site, when bound to phosphate, is in a closed state (see below) and that the positively charged cavity comprising K288, R290, and R291 is a site (other than the active site R263) that binds to one phosphorylated

(B) Ribbon depiction of the averaged minimized NMR structure of the phosphatase domain. Orientation of the structure and color-coding scheme for α helices and β strands in (A) and (B) are same.
(C) Ribbon diagram of the PAC-1 structure in a view opposite to that shown in (B), illustrating the structural elements of the enzymatic active site (orange). Side chains of the active site residues D226, C257S, and R263 are color-coded by atom type.
(D) Ribbon diagram of the crystal structure of the phosphatase domain of MKP-3, prepared with the structure coordinates obtained from the Protein Data Bank (ID code 1MKP). The orientation and color-coding for MKP-3 are similar to those used for PAC-1 in (C).
(E and F) Electrostatic potential surface representation of the PAC-1 phosphatase domain. Negatively charged residues, red; positively charged residues, blue. The orientation of the molecular surface representation in (E) and (F) is similar to that in (B) and (C), respectively. (A) was prepared by InsightII, (B), (C), and (D) were prepared with Ribbons [41], and (E) and (F) were prepared by GRASP [42].

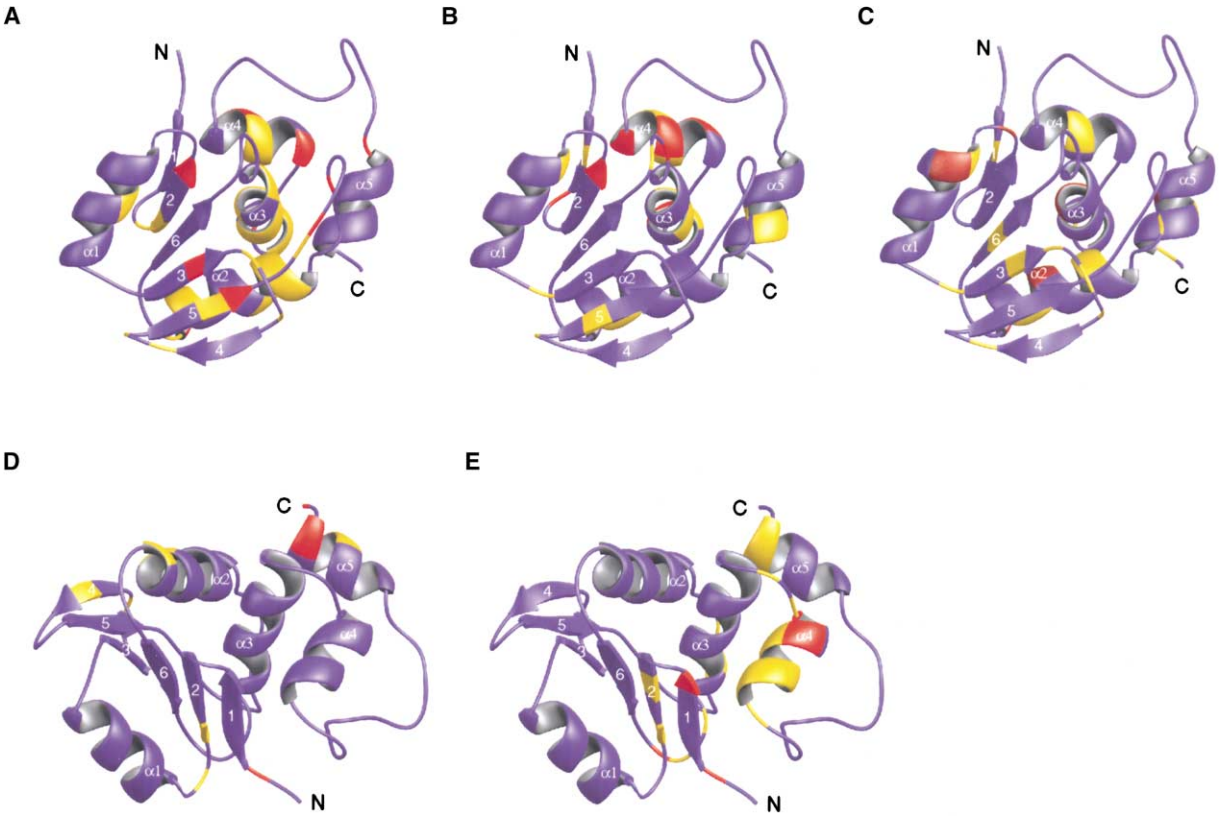

Figure 3. Molecular Interactions of the PAC-1 Phosphatase Domain

(A, B, and C) Ribbon diagrams of the phosphatase domain (residues 170–314), highlighting the residues that exhibited major resonance changes upon addition of phosphate (20 mM), *p*NPP (20 mM), or phosphorylated threonine (10 mM), respectively, to the protein sample in a 20 mM HEPES buffer of pH 7.2 containing 5 mM DTT-d_6 and 500 mM NDSB-201 (nondetergent sulfobetaines). NDSB-201, which does not affect the structure of the PAC-1 phosphatase domain, was used to enhance stability of the protein in the free form (without phosphate).

(D) Ribbon diagram of the PAC-1 phosphatase domain, illustrating the residues that underwent significant resonance changes in the NMR spectra upon addition of the MKP-3 kinase binding domain (residues 1–154).

(E) Ribbon diagram of the PAC-1 protein, showing the effect of the interdomain linker sequence (residues 131–169) on chemical shifts of the phosphatase domain (residues 170–314), based on the spectral comparison between the PAC-1 proteins consisting of residues 170–314 and 131–314. The protein residues are categorized into three groups according to the extent of chemical shift perturbation and are color-coded: red, large resonance shifts ($>$0.20 ppm); gold, medium changes (0.20–0.10 ppm); blue, small or no changes ($<$0.10 ppm). The results reflect the sum of the chemical shift changes of the backbone amide ^{1}H and ^{15}N resonances, as observed in the ^{15}N-HSQC spectra.

residue in EKR2. The latter seems to agree with the surface electrostatic potential of the molecule (Figure 2F). Since phosphotyrosine of the dual-phosphorylated ERK2 has been shown to be dephosphorylated first [25], it is conceivable that this newly discovered phosphate binding site is for phosphothreonine recognition. These results suggest direct and possibly simultaneous recognition of both phosphotyrosine and phosphothreonine at the active site of PAC-1.

Why does *p*NPP not bind to the enzyme active site? One possibility is that, when bound to phosphate, the active site is locked in a closed state, thus preventing it from binding to *p*NPP (K_D of $\sim$5 mM, as estimated by NMR titration). This explanation is consistent with the observations that (1) the β5–α2 loop is closer to the active site in the NMR structure (a closed state) than in the crystal structure (an apo state), (2) residues perturbed by phosphorylated threonine titration are in regions similar to those perturbed by *p*NPP binding (Figures 3B and 3C), and (3) the enzyme, under the same condition, showed little or negligible spectral changes upon addition of phosphorylated tyrosine (data not shown). It is important to note that the single-phosphorylated amino acids used in the NMR titration with the phosphatase domain were not ideal because of their positively charged amino, and negatively charged carboxyl, groups, which could interfere with enzyme and substrate recognition. Another possibility is that, even when bound to phosphate, the active site of PAC-1 is still structurally disengaged for coordinating a substrate for catalysis. A full substrate engagement would require conformational rearrangement of the enzyme active site through interactions between the two functional domains of PAC-1.

Interdomain Interactions

To address how the N-terminal kinase binding domain affects the active site conformation of the C-terminal phosphatase domain, we examined interdomain interactions. Because of the very low protein expression

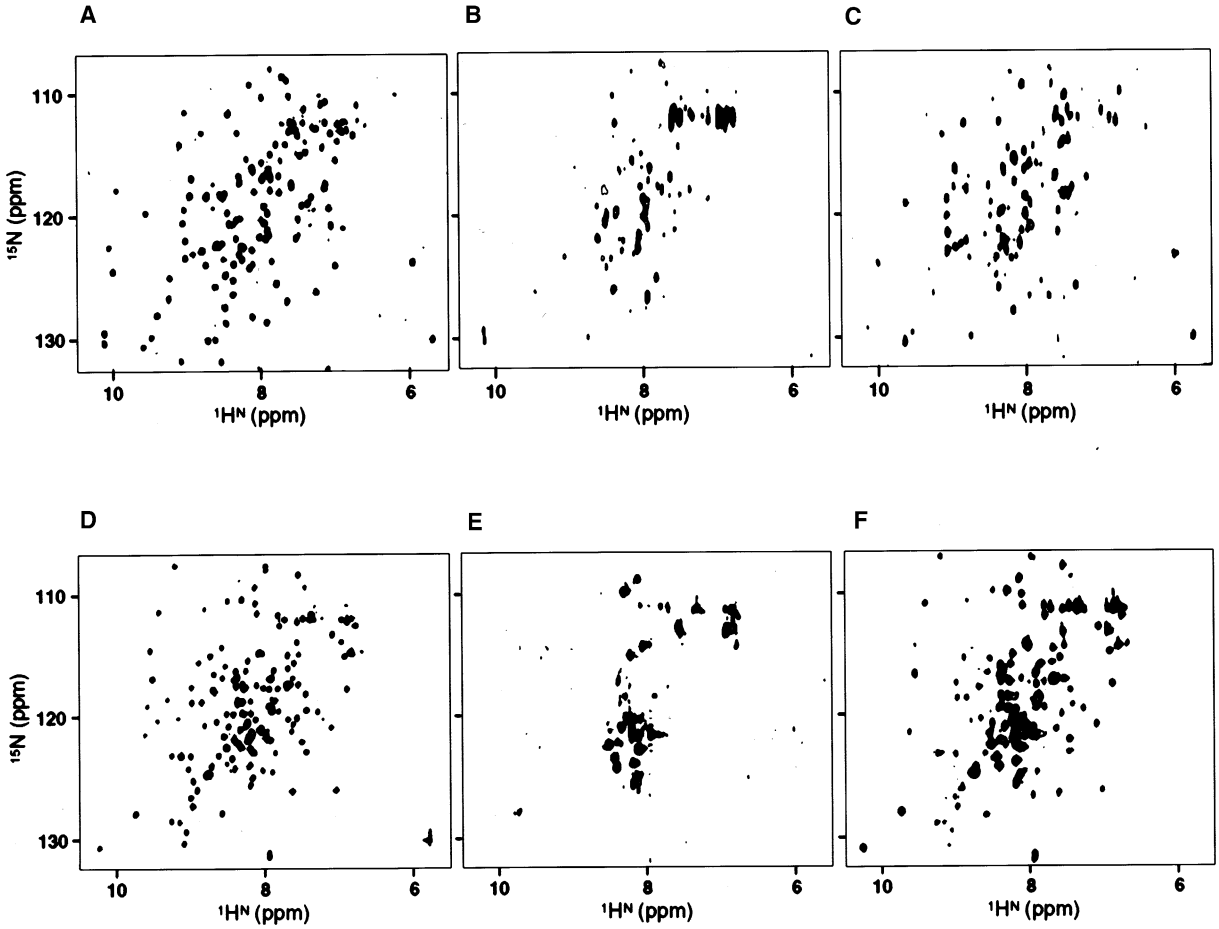

Figure 4. Protein Conformational Dynamics of the MKP Domains

Two-dimensional ^{15}N-HSQC spectra of the PAC-1 phosphatase domain (residues 170–314) collected in different conditions of (A) a 5 mM sodium phosphate buffer of pH 6.5 containing 5 mM DTT-d_{10} or (B) a 100 mM phosphate buffer of pH 6.5 containing 5 mM DTT-d_{10}.

(C) The PAC-1 phosphatase domain in the same buffer condition as that described in (B) plus a nonlabeled N-terminal kinse binding domain from MKP-3 (residues 1–154) (right panel). ^{15}N-HSQC spectrum of the MKP-3 N-terminal kinase binding domain (residues 1–154) collected in (D) a 100 mM sodium phosphate buffer of pH 6.5 containing 5 mM DTT-d_{10} and 200 mM urea or (E) in a 5 mM phosphate buffer of pH 6.5 containing 5 mM DTT-d_{10} and 200 mM urea.

(F) The MKP-3 protein in the same buffer condition as that described in (D) plus a nonlabeled C-terminal phosphatase domain from PAC-1 (residues 170–314). Note that the relatively low amount of urea, which showed no significant effect on the protein structure, as supported by NMR spectra, was used to stabilize the protein during NMR data collection.

level of the PAC-1 kinase binding domain, but its high sequence identity to that of MKP-3 (51% identity and additional 19% similarity), we used the N-terminal domain from MKP-3 (residues 1–154) and the C-terminal domain from PAC-1 in the NMR binding study. The key contact points between these two functional domains, as revealed from the NMR titration, are localized on one side of the phosphatase domain, away from the active site, involving β4, α2, and α5 (Figure 3D). To determine the role of the interdomain linker sequence, we further compared NMR spectra of PAC-1 consisting of residues 131–314 and 170–314. Binding of the linker sequence appears to occur on the back side of the phosphatase domain, almost directly behind the active site, involving α4, α5, β1, and β2 (Figure 3E). Residues in the phosphatase signature sequence of the β6-α3 loop and in α3 are also perturbed. These results confirm that the domain-domain interactions, via their linker sequence, may directly affect the active site geometry of the MKP.

The two MKP domains, although composed of compact tertiary structures, are highly dynamic in solution. For instance, the phosphatase domain of PAC-1 is in a stable conformation in a 5 mM sodium phosphate buffer of pH 6.5, as illustrated by its excellent ^{15}N-HSQC spectrum (uniform and narrow line width of protein amide resonance peaks) (Figure 4A). However, the protein resonances become significantly broadened when the phosphate concentration is increased to 100 mM (Figure 4B), indicating that the protein exists in multiple conformations that undergo an intermediate to fast exchange on the NMR timescale. Likewise, conformation of the kinase binding domain of MKP-3 is also dependent on buffer ionic strength—it is more stable in a high-ionic strength buffer than in a low-ionic strength buffer (Figures 4D and 4E). This buffer ionic strength dependence of conformational heterogeneity is reversible and was significantly diminished when the two domains were brought together (Figures 4C and 4F). Taken together,

these results argue that interdomain interactions between the two MKP functional domains are coupled to their functions.

Biological Implications

Dual-specific MKPs inactivate MAPKs that control mitogenic signal transduction in all eukaryotic organisms [1–3, 6, 7]. MKPs that consist of an N-terminal kinase binding domain and a C-terminal phosphatase domain exhibit very low phosphatase activity in the absence of substrates [15–19]. MKP binding to a selective MAPK results in activation of the phosphatase activity in a substrate-induced activation mechanism [20, 24, 25], rather than autoinhibition, commonly seen in other protein phosphatases [26]. Our new solution structure of the C-terminal phosphatase domain of PAC-1 and the identification of its interaction sites for the N-terminal kinase binding domain and for phosphotyrosine and phosphothreonine in the activated ERK2 represented here provide a key piece of knowledge toward full structural realization of the mechanism of action underlying MAPK-induced enzymatic activation of an MKP. In the absence of the substrate, the N-terminal kinase binding domain of an MKP is associated with its C-terminal phosphatase domain via the interdomain linker sequence, and the enzyme exists in a low-activity state because of disengagement of its active site residues. Alteration of the cooperative interdomain interactions of an MKP resulting from its N-terminal domain binding to an MAPK allosterically triggers conformational rearrangement of the phosphatase active site for specific recognition of the MAPK's dual-phosphorylation sequence, leading to enzymatic activation of the MKP to a high-activity state that is essential for dephosphorylation and inactivation of the MAPK. This dynamic coupling of MAPK inactivation to MAPK substrate-induced activation of an MKP provides a tightly controlled regulation that enables these two key enzymes to keep each other in check and thereby guarantees the fidelity of intracellular signal transduction.

Experimental Procedures

Sample Preparation

cDNA sequences encoding the phosphatase domain of PAC-1 consisting of residues 131–314 or 170–314 were subcloned into a pET15b expression vector (Novagen), which produces the recombinant protein with a hexahistidine (His_6) sequence at the N terminus. The enzymatic nucleophile C257 in the phosphatase domain was mutated to serine for the NMR structural study. The proteins were overexpressed in *Escherichia coli* BL21(DE3) cells. Uniformly ^{15}N- and $^{15}N/^{13}C$-labeled proteins were prepared by growing bacteria at 37°C in an M9 minimal medium containing $^{15}NH_4Cl$ with or without $^{13}C_6$-glucose in H_2O or 75% ^2H_2O. Protein induction was conducted at 25°C for about 4 hr with 0.3 mM IPTG (isopropylthio-β-D-galactoside). The phosphatase domain was purified by affinity chromatography on a Hi-Trap nickel column (Pharmacia) and then by cleavage of the His_6 tag with thrombin treatment. The cleaved protein was further purified by ion exchange chromatography. NMR samples contained the protein of 0.5 mM in a 5 mM sodium phosphate buffer of pH 6.5 containing 5 mM DTT-d_{10} in $H_2O/^2H_2O$ (9:1) or ^2H_2O. The N-terminal kinase binding domain of MKP-3 was prepared according to a procedure described previously [20]. The activated and dual-phosphorylated ERK2 was prepared by its coexpression with a constitutively active MEK1 R4F in *E. coli* BL21(DE3) cells and purified with procedures previously reported [32, 33].

NMR Spectroscopy

All NMR spectra were acquired at 25°C on a 600 MHz or 500 MHz Bruker DRX NMR spectrometer. ^1H, ^{13}C, and ^{15}N resonances of the protein were assigned with standard deuterium-decoupled triple-resonance spectra of HNCA, HN(CO)CA, HN(CA)CB, HN(COCA)CB, and (H)C(CO)NH-TOCSY [30, 34], recorded on a uniformly $^{15}N/^{13}C$-labeled and fractionally deuterated protein. The side chain assignments were completed with 3D HCCH-TOCSY [35] data collected from a uniformly $^{15}N/^{13}C$-labeled protein. NOE-derived distance restraints were obtained from ^{15}N- or ^{13}C-edited 3D NOESY spectra [35]. ϕ angle restraints were determined from $^3J_{HN,H\alpha}$ coupling constants measured in a 3D HNHA-*J* spectrum [35]. Slowly exchanging amide protons were identified from a series of 2D ^{15}N-HSQC spectra recorded after the H_2O buffer was changed to ^2H_2O buffer. All NMR spectra were processed with NMRPipe [36] and analyzed with NMRView [37].

Structure Calculations

Structures of the PAC-1 protein were calculated with a distance geometry simulated-annealing protocol with X-PLOR [38]. Initial structure calculations were done with manually assigned NOE-derived distance restraints. Hydrogen bond distance restraints were added at the late stage of structure calculations for residues with characteristic NOE patterns. The converged structures were then used for the iterative automated assignment of the NOE spectra by ARIA [39], which integrates with X-PLOR for the structure refinement. The final structure calculations employed a total of 2138 NOE-derived distance restraints obtained from the manual and ARIA-assisted assignments from the ^{15}N- or ^{13}C-edited NOE data. The NOE-derived restraints were categorized on the basis of the observed NOE peak intensities. Additionally, 110 hydrogen bond distance restraints for 55 hydrogen bonds and 126 ϕ and ψ angle restraints, determined from the 3D HNHA-*J* experiment and TALOS program [40], were also used in the calculations. For the final 20 lowest-energy NMR structures, no distance or torsional angle restraint was violated by more than 0.5 Å or 5°, respectively (Table 1).

Protein Binding

Protein-protein and protein-ligand binding studies were performed by recording a series of 2D ^1H-^{15}N HSQC spectra on the uniformly ^{15}N-labeled PAC-1 phosphatase domain (0.2 mM) with and without the MKP-3 N-terminal kinase binding domain (0.20–0.50 mM), phosphate, *p*-nitrophenyl phosphate, or ERK2 peptides. The protein samples were prepared in the same aqueous buffer containing 5–100 mM sodium phosphate and 5 mM perdeuterated DTT-d_{10} at pH 6.5. The GST fusion proteins (5 μM) of PAC-1 C257S mutant or the full-length MKP-3 C299S mutant bound to the glutathione Sepharose beads (Amersham Biosciences) were incubated with the purified, activated, and dual-phosphorylated ERK2 (20 μM) in 50 mM sodium phosphate buffer of pH 6.5 containing 150 mM NaCl and 1 mM DTT at 25°C for 30 min and then at 4°C for 2 hr. The glutathione Sepharose beads (10 μl) were washed extensively with the phosphate buffer. Proteins eluted from the Sepharose beads were separated by SDS-PAGE and visualized by Western blotting with anti-GST antibody (Pierce) or anti-histidine tag antibody (Amersham) and alkaline phosphatase-conjugated donkey anti-mouse IgG (Promega). The dual-phosphorylation state of ERK2 was confirmed by Western blotting with anti-pT^{183} ERK1/2, anti-ACTIVE ($pT^{183}EpY^{185}$) ERK1/2, and anti-pY antibodies (Promega).

Acknowledgments

We thank K. Kelly and M. Cobb for providing cDNA constructs of PAC-1 and ERK2, respectively, and S. Shimotakahara and K.S. Yan for technical advice and support. A.F. is a recipient of a Wellcome Trust Postdoctoral Fellowship. The work was supported by a grant from the National Institutes of Health to M.-M.Z.

Received: August 6, 2002
Revised: November 15, 2002
Accepted: November 15, 2002

References

1. Chang, L., and Karin, M. (2001). Mammalian MAP kinase signaling cascades. Nature *410*, 37–40.
2. Lewis, T.S., Shapiro, P.S., and Ahn, N.G. (1998). Signal transduction through MAP kinase cascades. Adv. Cancer Res. *74*, 49–139.
3. Robinson, M.J., and Cobb, M.H. (1997). Mitogen-activated protein kinase pathways. Curr. Opin. Cell Biol. *9*, 180–186.
4. Robbins, D.J., Zeng, E., Owaki, H., Vanderbilt, C.A., Ebert, D., Geppert, T.D., and Cobb, M.H. (1993). Regulation and properties of extracellular signal-regulated protein kinases 1 and 2 in vitro. J. Biol. Chem. *268*, 5097–5106.
5. Payne, D.M., Rossomando, A.J., Martino, P., Erickson, A.K., Her, J.-H., Shabanowitz, J., Hunt, D.F., Weber, M.J., and Sturgill, T.W. (1991). Identification of the regulatory phosphorylation sites in pp42/mitogen-activated protein kinases (MAP kinases). EMBO J. *10*, 885–892.
6. Keyse, S.M. (2000). Protein phosphatases and the regulation of mitogen-activated protein kinase signalling. Curr. Opin. Cell Biol. *12*, 186–192.
7. Camps, M., Nichols, A., and Arkinstall, S. (1999). Dual specificity phosphatases: a gene family for control of MAP kinase function. FASEB J. *14*, 6–16.
8. Cano, E., and Mahadevan, L. (1995). Parallel signal processing among mammalian MAPKs. Trends Biochem. Sci. *20*, 117–122.
9. Marshall, C.J. (1995). Specificity of receptor tyrosine kinase signaling: transient versus sustained extracellular signal-regulated kinase activation. Cell *80*, 179–185.
10. Ward, Y., Gupta, S., Jensen, P., Wartmann, M., Davis, R.J., and Kelly, K. (1994). Control of MAP kinase activation by the mitogen-induced threonine/tyrosine phosphatase PAC1. Nature *367*, 651–654.
11. Rohan, P.J., Davis, P., Moskaluk, C.A., Kearns, M., Krutzsch, H., Siebenlist, U., and Kelly, K. (1993). PAC-1: a mitogen-induced nuclear protein tyrosine phosphatase. Nature *259*, 1763–1766.
12. Muda, M., Boschert, U., Dickinson, R., Martinou, J.-C., Martinou, I., Camps, M., Schlegel, W., and Arkinstall, S. (1996). MKP-3, a novel cytosolic protein-tyrosine phosphatase that examplifies a new class of mitogen-activated protein kinase phosphatase. J. Biol. Chem. *271*, 4319–4326.
13. Muda, M., Theodosiou, A., Rodrigues, N., Boschert, U., Camps, M., Gillieron, C., Davies, K., Ashworth, A., and Arkinstall, S. (1996). The dual specificity phosphatase M3/6 and MKP-3 are highly selective for inactivation of distinct mitogen-activated protein kinases. J. Biol. Chem. *271*, 27205–27208.
14. Groom, L.A., Sneddon, A.A., Aleesi, D.R., Down, S., and Keyse, S.M. (1996). Differential regulation of the MAP, SAP and RK/p38 kinases by Pyst1, a novel cytosolic dual-specificity phosphatase. EMBO J. *15*, 3621–3632.
15. Muda, M., Theodosiou, A., Gilleron, C., Smith, A., Chabert, C., Camps, M., Boschert, U., Rodrigues, N., Davis, K., Ashworth, A., et al. (1998). The mitogen-activated protein kinase phosphatase-3 N-terminal noncatalytic region is responsible for tight substrate binding and enzymatic specificity. J. Biol. Chem. *273*, 9323–9329.
16. Camps, M., Nichols, A., Gillieron, C., Antonsson, B., Muda, M., Chabert, C., Boschert, U., and Arkinstall, S. (1998). Catalytic activation of the phosphatase MKP-3 by ERK2 mitogen-activated protein kinase. Science *280*, 1262–1265.
17. Chen, P., Hutter, D., Yang, X., Gorospe, M., Davis, R.J., and Liu, Y. (2001). Discordance between the binding affinity of mitogen-activated protein kinase subfamily members for MAP kinase phosphatase-2 and their ability to activate the phosphatase catalytically. J. Biol. Chem. *276*, 29440–29449.
18. Hutter, D., Chen, P., Barnes, J., and Liu, Y. (2000). Catalytic activation of mitogen-activated protein (MAP) kinase phosphatase-1 by binding to p38 MAP kinase: critical role of the p38 C-terminal domain in its negative regulation. Biochem. J. *352*, 155–163.
19. Slack, D.N., Seternes, O.M., Gabrielsen, M., and Keyse, S.M. (2001). Distinct binding determinants for ERK2/p38alpha and JNK map kinases mediate catalytic activation and substrate selectivity of map kinase phosphatase-1. J. Biol. Chem. *276*, 16491–16500.
20. Farooq, A., Chaturvedi, G., Mujtaba, S., Plotnikova, O., Zeng, L., Dhalluin, C., Ashton, R., and Zhou, M.-M. (2001). Solution structure of ERK2 binding domain of MAPK phosphatase MKP-3: structural insights into MKP-3 activation by ERK2. Mol. Cell *7*, 387–399.
21. Tanoue, T., Adachi, M., Moriguchi, T., and Nishida, E. (2000). A conserved docking motif in MAP kinases common to substrates, activators and regulators. Nat. Cell Biol. *2*, 110–116.
22. Nichols, A., Camps, M., Gillieron, C., Chabert, C., Brunet, A., Wilsbacher, J., Cobb, M., Pouyssegur, J., Shaw, J.P., and Arkinstall, S. (2000). Substrate recognition domains within extracellular signal-regulated kinase mediate binding and catalytic activation of mitogen-activated protein kinase phosphatase-3. J. Biol. Chem. *275*, 24613–24621.
23. Zhou, B., Wu, L., Shen, K., Zhang, J., Lawrence, D.S., and Zhang, Z.-Y. (2001). Multiple regions of MAP kinase phosphatase 3 are involved in its recognition and activation by ERK2. J. Biol. Chem. *276*, 6506–6515.
24. Fjeld, C.C., Rice, A.E., Kim, Y., Gee, K.R., and Denu, J.M. (2000). Mechanistic basis for catalytic activation of mitogen-activated protein kinase phosphatase 3 by extracellular signal-regulated kinase. J. Biol. Chem. *275*, 6749–6757.
25. Zhao, Y., and Zhang, Z.Y. (2001). The mechanism of dephosphorylation of extracellular signal-regulated kinase 2 by mitogen-activated protein kinase phosphatase 3. J. Biol. Chem. *276*, 32382–32391.
26. Hof, P., Pluskey, S., Dhe-Paganon, S., Eck, M.J., and Shoelson, S.E. (1998). Crystal structure of the tyrosine phosphatase SHP-2. Cell *92*, 441–450.
27. Stewart, A.E., Dowd, S., Keyse, S.K., and mcDonald, N.Q. (1999). Crystal structure of the MAPK phosphatase Pyst1 catalytic domain and implications for regulated activation. Nat. Struct. Biol. *6*, 174–181.
28. Jia, Z., Barford, D., Flint, A.J., and Tonks, N.K. (1995). Structural basis for phosphotyrosine peptide recognition by protein tyrosine phosphatase 1B. Science *268*, 1754–1758.
29. Salmeen, A., Andersen, J.N., Myers, M.P., Tonks, N.K., and Barford, D. (2000). Molecular basis for the dephosphorylation of the activation segment of the insulin receptor by protein tyrosine phosphatase 1B. Mol. Cell *6*, 1–12.
30. Sattler, M., Schleucher, J., and Griesinger, C. (1999). Heteronuclear multidimensional NMR experiments for the structure determination of proteins in solution employing pulsed field gradients. Prog. NMR Spectrosc. *34*, 93–158.
31. Rigas, J.D., Hoff, R.H., Rice, A.E., Hengge, A.C., and Denu, J.M. (2001). Transition state analysis and requirement of Asp-262 general acid/base catalyst for full activation of dual-specificity MKP3 by extracellular regulated kinase. J. Biol. Chem. *40*, 4398–4406.
32. Khokhlatchev, A., Xu, S., English, J., Wu, P., Schaefer, E., and Cobb, M.H. (1997). Reconstitution of MAP kinase phosphorylation cascades in bacteria: efficient synthesis of active protein kinases. J. Biol. Chem. *272*, 11057–11062.
33. Canagarajah, B.J., Khokhlatchev, A., Cobb, M.H., and Goldsmith, E.J. (1997). Activation mechanism of the MAP kinase ERK2 by dual phosphorylation. Cell *90*, 859–869.
34. Yamazaki, T., Lee, W., Arrowsmith, C.H., Mahandiram, D.R., and Kay, L.E. (1994). A suite of triple resonance NMR experiments for the backbone assignment of ^{15}N, ^{13}C, ^{2}H labeled proteins with high sensitivity. J. Am. Chem. Soc. *116*, 11655–11666.
35. Clore, G.M., and Gronenborn, A.M. (1994). Multidimensional heteronuclear nuclear magnetic resonance of proteins. Methods Enzymol. *239*, 349–363.
36. Delaglio, F., Grzesiek, S., Vuister, G.W., Zhu, G., Pfeifer, J., and Bax, A. (1995). NMRPipe: a multidimensional spectral processing system based on UNIX pipes. J. Biomol. NMR *6*, 277–293.
37. Johnson, B.A., and Blevins, R.A. (1994). NMRView: a computer program for the visualization and analysis of NMR data. J. Biomol. NMR *4*, 603–614.
38. Brunger, A.T. (1993). X-PLOR Version 3.1: A System for X-Ray Crystallography and NMR, Version 3.1 Edition (New Haven, CT: Yale University Press).

39. Nilges, M., and O'Donoghue, S. (1998). Ambiguous NOEs and automated NOE assignment. Prog. NMR Spectroscopy *32*, 107–139.
40. Cornilescu, G., Delaglio, F., and Bax, A. (1999). Protein backbone angle restraints from searching a database for chemical shift and sequence homology. J. Biomol. NMR *13*, 289–302.
41. Carson, M. (1991). Ribbons 2.0. J. Appl. Crystallogr. *24*, 958–961.
42. Nicholls, A., Bharadwj, R., and Honig, B. (1993). GRASP: graphical representation and analysis of surface properties. Biophys. J. *64*, 166–170.

Accession Numbers

The atomic coordinates of the PAC-1 phosphatase domain structure have been deposited in the Protein Data Bank under ID code 1M3G.